

Modelling of the Performance of a Building-Mounted Ducted Wind Turbine

This article has been downloaded from IOPscience. Please scroll down to see the full text article.

2007 J. Phys.: Conf. Ser. 75 012001

(<http://iopscience.iop.org/1742-6596/75/1/012001>)

View [the table of contents for this issue](#), or go to the [journal homepage](#) for more

Download details:

IP Address: 117.204.85.235

The article was downloaded on 23/05/2011 at 17:19

Please note that [terms and conditions apply](#).

Modelling of the Performance of a Building-Mounted Ducted Wind Turbine

S J Watson, D G Infield, J P Barton and S J Wylie

Centre for Renewable Energy Systems Technology, Department of Electronic and Electrical Engineering, Loughborough University, Ashby Road, Loughborough, Leicestershire, LE11 3TU, United Kingdom

s.j.watson@lboro.ac.uk

Abstract. This paper presents computational fluid dynamics (CFD) modelling of the performance of a building-mounted ducted wind turbine. A resistive volume within the duct is used to represent a cross-flow turbine and different diffuser geometries have been investigated. A comparison is made between the power performance ratio of such a building-mounted ducted wind turbine rotor predicted by CFD calculations and those predicted on the basis of one-dimensional (1D) theory. Good agreement is seen between the two approaches for a free-standing duct but deviations are seen for the building-mounted case for the calculated power performance ratio apparently due to asymmetry in the flow profile entering the duct and the flow geometry around the combination of building and duct.

1. Introduction

There has been an increasing interest in the installation of wind turbines within the built environment on and around buildings in order to help meet increasing demands for energy and targets for renewable energy generation. A number of small turbines reputedly suited to such applications have been proposed including free-yawing up- and down-wind horizontal axis turbines [1], [2], vertical axis turbines [3] and cross-flow turbines [4]. Although sparse, some research has been undertaken to assess the expected yield from such turbines [5], [6], [7], but almost nothing has been published on building-integrated wind turbines. This paper presents an assessment of the expected power output and energy yield from a hypothetical cross-flow wind turbine placed in a diffusing duct on a flat-roof building in an urban environment.

First, a brief review of ducted wind turbine research is presented. Following this, the paper describes in outline a 1D model developed to calculate the power output of a rotor in a duct. The main section of the paper describes CFD results from a commercial package ANSYS CFX 10 used to model the wind flow through a hypothetical duct with various rotor area to outlet area ratios and for a range of resistances within the duct representing a cross-flow wind turbine rotor. Finally, a comparison is made between the CFD and 1D model results and any differences discussed.

2. Ducted Wind Turbine

Some earlier research work on the effect of diffusers and augmenters for wind turbine rotors is available. The basic principle behind the use of a diffuser is to obtain a higher energy density at a rotor than would be seen in a free moving fluid (either air or water). This then allows:

- The generation of increased power from a given rotor diameter;
- The generation of increased power from a given area of fluid stream.

The second of these is most relevant for a tidal stream device and the first is of most relevance for wind turbines. The economic motivation is the savings potentially achieved through reduction in the size and cost of the rotor for a given power output.

The research work in this field has taken a number of approaches in studying the effect of diffusers, namely:

- Simple semi-empirical models;
- Computational fluid dynamics;
- Wind tunnel tests;
- Full or partial-scale outdoor tests.

In ref. [9], CFD simulations of flow through a free (i.e. not building-mounted) ducted diffuser were analysed. These showed:

- That the optimum angle of diffusion was 6° ;
- That increasing the duct length increased the wind speed up to a point, but then flattened off (at around 2-3 times the duct diameter);
- That adding a flange to the outlet of the duct increased optimum wind speed up from 1.4 to 1.7;
- The size of the flange did not make much difference.

These CFD simulations were then compared with field experiments carried out with a ducted turbine. The duct had an expansion angle of 4° and a flange at the outlet. When the turbine was allowed to yaw, the increase in production of the ducted turbine over that in the free stream was found to be 1.16. When the turbine was fixed (no yaw), the increase in output was found to be 1.65. This was much lower than the predicted factor of around 5, but the authors point out that the theoretical calculations were for a case with no rotor and that frequent and rapid changes in wind direction degraded performance. It is interesting that the estimate given in [8] of 30% was in the middle of the range for the yawing and fixed configuration.

Ref. [10] looked at the performance of a flanged diffuser using a combination of CFD modelling and wind tunnel tests. This confirmed the assertion in [9] that a flange can significantly enhance performance. It was also seen that a relatively low rotor resistance was required in order to maximise wind speed-up within the duct. It was stated in this paper that a duct angle of 4° was expected to optimise performance before flow separation would be expected to occur. Experiments were done with a diffuser at a 15° angle which showed a reduced speed-up at low turbine resistance, but at higher loading the drop-off in the performance was less than for a 4° diffuser. It was proposed that for the highly loaded case, the flow re-attached to the wall of the diffuser which would explain the better performance in this case. Notably, it was found that the base pressure coefficient was very important in determining the performance of the flanged duct.

A related group [11] looked at another flanged diffuser with an actual wind turbine within the duct and without the duct. Once again, CFD calculations (with a load) were compared with the experimental measurements in a wind tunnel. This time the flanged diffuser has a 12° angle. The power coefficient for the ducted wind turbine was found to be about four times as high as the bare turbine. When normalised to the actual wind speed immediately upstream of the rotor, the performance was found to be identical. This would imply that the enhancement of performance was solely due to speed-up of wind approaching the turbine due to the diffuser. Interestingly, it was noted that the vortex structure downstream of the rotor differed markedly for the shrouded and unshrouded cases. It was seen with the turbine in the duct that the vortex structure was rapidly destroyed, but in the bare case, vortex structures were apparent far downstream.

Results from a CFD simulation made in [12] show that the power of a wind turbine within a shrouded diffuser can be increased by a factor of over 5, though this was not verified against any

experimental results. It was unclear what the angle of the diffuser was in this case, as it had a sail wing profile increasing in angle from the throat to the outlet.

One group [13] has looked at a ducted wind turbine integrated into a building taking advantage of the pressure drop between the face of a building and the top of the building. Their results suggested wind speeds of up to 30% higher than in the approaching free-stream could be induced in the duct. This duct did not have any degree of augmentation or diffusion.

To date, there appears to be no research work reported on the performance of an augments or diffuser situated on top of a flat-roof building.

3. One-Dimensional Model

Ref. [8] gives a good review of the principles behind ducted turbines, developing a one-dimensional (1D) model which allows for the optimisation of the performance of a free-standing duct with contracting inlet and diffusing outlet as shown in Figure 1. A formula has been derived for the power performance coefficient, C_p :

$$C_p = \eta_t K \left(\frac{\eta_{01} - C_{P_b}}{\eta_{01} + K - C_{P_{23}}} \right)^{3/2} \quad (1)$$

where η_t is the efficiency of the turbine, K is the resistance coefficient for the rotor in the duct given by:

$$K \equiv \frac{P_1 - P_2}{\frac{1}{2} \rho U_1^2} \quad (2)$$

and P_1 and P_2 are the static pressures immediately upstream and downstream of the rotor, respectively, U_1 is the one-dimensional wind speed immediately upstream of the rotor and ρ is the air density. The base pressure coefficient due to the pressure drop created due to the overall blockage effect of the duct, C_{P_b} , is given by:

$$C_{P_b} = \frac{P_3 - P_0}{\frac{1}{2} \rho U_0^2} \quad (3)$$

where P_0 is the static free-stream pressure upstream of the duct, P_3 is the static pressure at the duct outlet and U_0 is the one-dimensional free-stream wind speed approaching the duct. The diffuser pressure coefficient out of the duct, $C_{P_{23}}$ is given by:

$$C_{P_{23}} = \frac{P_3 - P_2}{\frac{1}{2} \rho U_1^2} \equiv \eta_{23} \left\{ 1 - \left(\frac{U_3}{U_1} \right)^2 \right\} \quad (4)$$

where U_3 is the one-dimensional wind speed at the duct outlet.

There is a similar pressure coefficient for flow into the duct, $C_{P_{01}}$:

$$C_{P_{01}} = \frac{P_1 - P_0}{\frac{1}{2} \rho U_0^2} \equiv \eta_{01} \left\{ 1 - \left(\frac{U_1}{U_0} \right)^2 \right\} \quad (5)$$

where η_{01} and η_{23} are diffusion efficiencies into and out of the duct, respectively. These values represent how efficiently fluid is pulled into the entrance and out of the exit to the duct without pressure gradient losses due to flow separation, friction, etc.

From continuity:

$$\frac{U_3}{U_1} = \frac{A_1}{A_3} \quad (6)$$

And

$$\frac{U_1}{U_0} = \frac{A_{0i}}{A_1} \quad (7)$$

where A_{0i} is the area of the duct inlet, A_1 is the area of the duct immediately upstream of the turbine and A_3 is the area of the duct outlet. Note that $U_2 = U_1$ and $A_2 = A_1$ where U_2 is the wind speed immediately downstream of the rotor and A_2 is the area of the duct immediately downstream of the rotor.

With values determined from experiments for C_{P_b} , $C_{P_{23}}$ and $C_{P_{01}}$ is it possible to estimate the performance of a duct with varying degrees of resistance K using equations 1, 5 and 4.

Application of these equations for cases where the area ratios A_2/A_3 ranged between 0.25 and 0.5 showed that for a duct with high inlet and outlet efficiencies, i.e. $\eta_{01} = 1$, $\eta_{23} = 0.8$, a maximum power coefficient greater than the Betz limit (0.593) from actuator disc theory is achieved with a value of K around 0.5 (a relatively low resistance turbine), although it should be noted that this is referenced to the *rotor area*, not the duct size.

This theory was compared with experimental measurements and showed that there was little to be gained by controlling diffusion at the inlet, but that efficiently controlled diffusion at the outlet could give rise to a 30% power enhancement compared with a turbine in the free-stream. It was also concluded that if turbine rotational speed needed to be high due to the requirements of the generator, that the blades of the rotor should be highly pitched and lightly loaded (at least for a propeller type turbine).

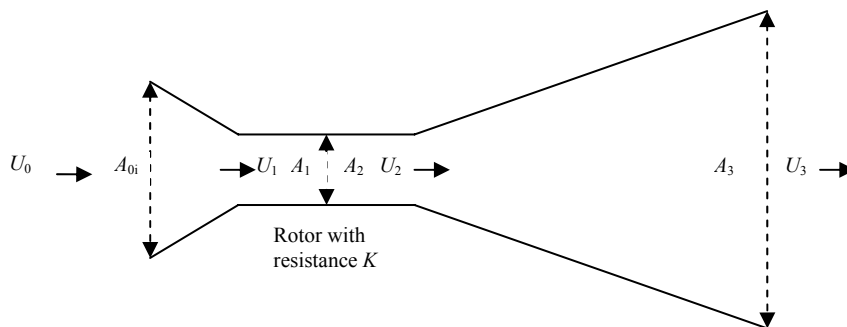


Figure 1: Schematic diagram of duct with contracting inlet and diffusing outlet and resistance to simulate a rotor at the throat.

4. CFD Modelling of Duct Performance

4.1. Model Set-Up

The flow around both a building-mounted and free-standing duct with a resistive volume within the duct to represent a cross-flow wind turbine was computed using the Reynolds Averaged Navier Stokes (RANS) equations implemented in the commercial CFD software ANSYS CFX. ANSYS CFX is based on a coupled solver for mass and momentum and uses an algebraic multi-grid algorithm for convergence acceleration. The numerical scheme is a co-located pressure based method for all Mach numbers. A Rhie-Chow interpolation scheme [14] is used to locate the solution of the pressure and velocity fields at the same nodal locations in the mesh. Due to the impracticality of modelling the turbulent structure close to the ground, wall functions are used to model the mean wind profile and

turbulent kinetic energy. The model was run using the SST ($k-\omega$) turbulence model [15] which has been shown to predict flow separation within diffusers with a better accuracy than the commonly used $k-\epsilon$ turbulence model [16]. The model was run in a steady state mode.

Figure 2 shows a schematic of the building and duct modelled using ANSYS CFX. To reduce computational time, only half the duct and building were modelled assuming a symmetry plane at one wall passing through the centre of the building and duct. The building has a half-width of 25m, height of 20m, and a length of 14m. The duct has a half-width of 5m and height of 3m. The domain was made large enough so that the walls of the domain did not influence the flow close to the building with an inlet having a half-width of 130m metres and a height of 100m. The domain extends 300m in the direction of wind flow and the inlet is 100m from the building. The entrance to the duct as shaped as far as possible to smooth the flow into the duct.

A free slip boundary condition was implemented at the top and side walls of the domain. A 5 m/s uniform vertical profile wind speed was set entering the inlet with constant static pressure at the outlet to the domain. Note that this is a simplification, as in reality there will be a significant wind shear in the urban environment which will tend to reduce the wind speed-up over a real building.

The no slip boundary condition was implemented at the ground and the surfaces of the building and duct. An unstructured tetrahedral mesh was used with the finest resolution (down to 2mm) close to regions where the greatest changes in wind speed and pressure gradient were expected, i.e. at the building edges and within the duct, and with a coarser resolution at the outer walls of the domain (up to a few metres). Close to the ground and surfaces of the building and duct, the mesh was extruded as an inflation layer to more accurately model the flow which would be parallel to the surfaces.

Within the duct at the point of maximum contraction, a sub-domain of a cylindrical volume shape was created to represent a cross-flow wind turbine rotor. It was impractical to model the aerodynamic effect of the rotor blades, so momentum extraction was simulated by giving the cylindrical volume resistance to the flow in the form of a thrust term where the thrust could be varied corresponding to differing degrees of resistance K corresponding to the 1D modeling.

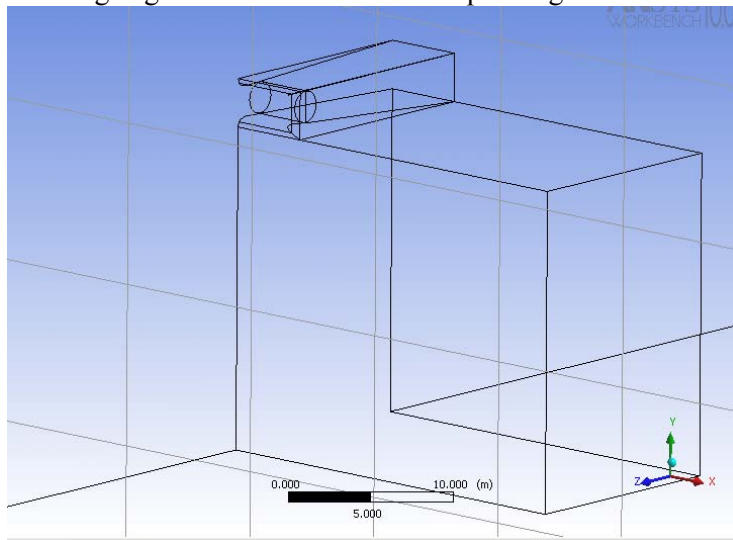


Figure 2: The duct and building modelled using ANSYS CFX. There is a symmetry plane through the centre of the duct and building.

4.2. Results

A number of CFD simulations were carried out for three different contraction ratios ($A_3/A_1=1.9, 3.75$ and 6.6), several simulated rotor resistances K , and a full-span and half span duct. The rectangular duct has an internal contraction in both the vertical and lateral directions as seen in Figure 2.

Figure 3 (a) and (b) show streamline plots for the full span duct for low resistance and high resistance cases, respectively, for the case where $A_3/A_1=1.9$. The structure of the streamlines is broadly similar, with a lower overall wind speed for the high resistance case and some flow separation in the bottom of the duct. The wind speed shows significant vertical shear in both cases.

Figure 4 (a) and (b) show streamline plots for the half span duct for low resistance and high resistance cases respectively, again for the case where $A_3/A_1=1.9$. The half-span duct, as the name suggests, only spans half the length of the building. This time, the low resistance case shows significant flow separation, however, in the high resistance case, the separation is almost eliminated. This would appear to be due to the greater resistance of the rotor in the centre than at the edges forcing the flow towards the walls inhibiting separation. Figure 5 shows how the power performance coefficient C_p varies as a function of resistance K for the case where $A_3/A_1=1.9$ comparing the full duct with the half duct. The peak performance is reached for a K of slightly greater than 1. It can be seen that at very low resistance, the full span has a greater efficiency than the half-span case, however, as resistance increases, the half-span duct becomes more efficient. This is consistent with the inhibiting of flow separation and increase in efficiency of the duct is noted above from Figure 4.

The difference between the half-duct and the full duct case would seem to be due to a greater duct diffusion angle, i.e. 6° for the half-span duct compared with 3° for the full-span duct, and a different flow geometry, i.e. in the full-span case there is a large flow separation bubble behind the building with upward flow directly interacting with the flow exiting from the duct which is pushing the exiting flow upward and encouraging separation from the bottom of the duct. In the half-span case, there is a much smaller area of re-circulating flow behind the duct on top of the building which can be more easily inhibited by the forcing of flow to the edges of the duct by a higher resistance rotor.

Figure 6 shows the vertical wind shear in the duct just upstream of the rotor for the different contraction ratios and the full duct/half cases in the case of low resistance. It can be seen that the profiles in all cases are far from uniform. The degree of profile asymmetry is greatest for the $A_3/A_1=1.9$ contraction ratio cases and especially, the half-span duct case.

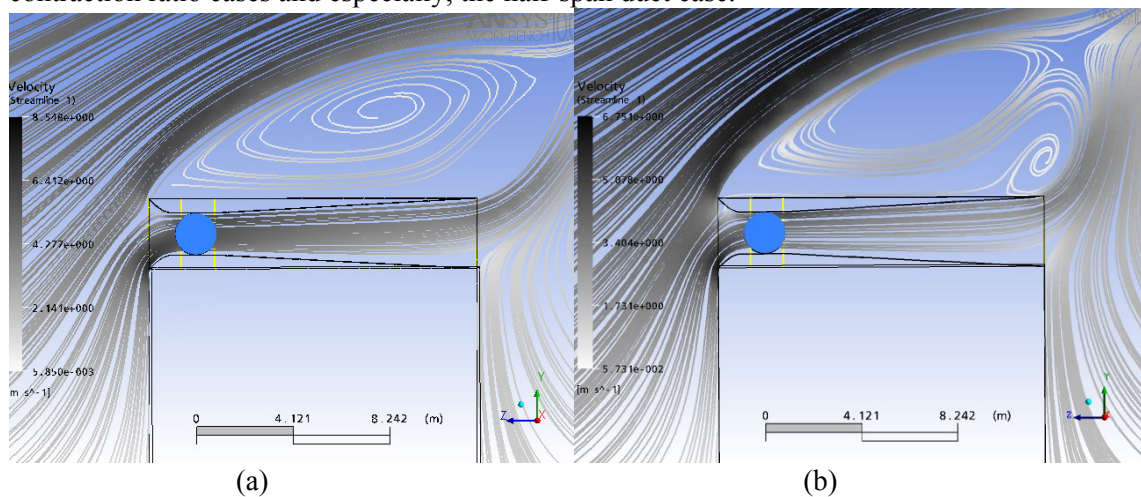


Figure 3: Streamlines for flow through full-span duct with $A_3/A_1=1.9$ with (a) $K=0.38$, (b) $K=1.33$.

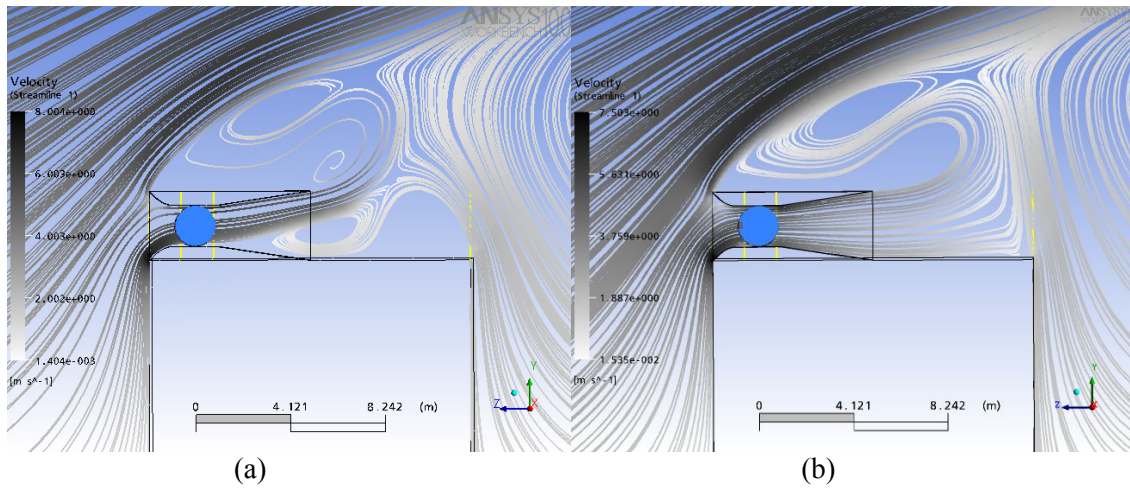


Figure 4: Streamlines for flow through half-span duct with $A_3/A_1=1.9$, with (a) $K=0.36$, (b) $K=1.29$.

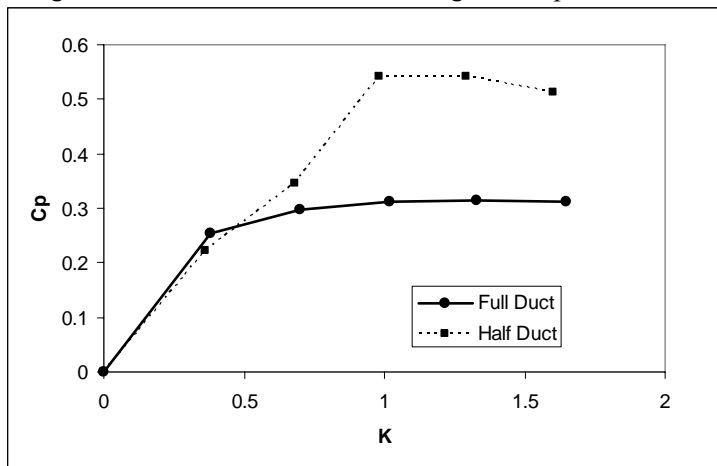


Figure 5: Power coefficient C_p as a function of resistance K for the full-span duct and half-span duct where $A_3/A_1=1.9$.

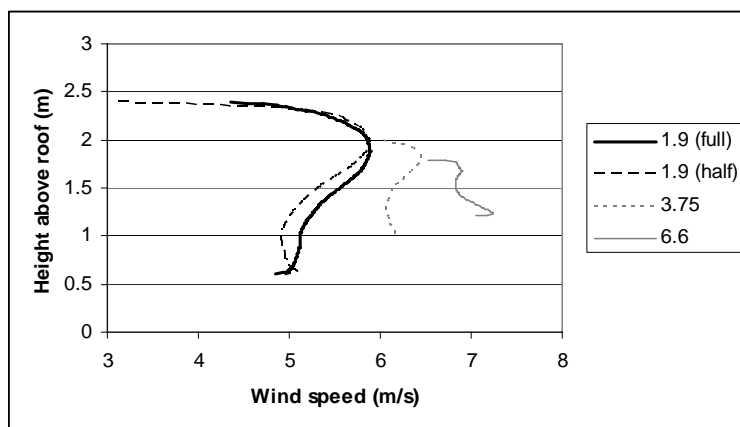


Figure 6: Comparison of vertical wind speed profiles within ducts of different contraction ratios just upstream of the rotor. $K=0.38$ ($A_3/A_1=1.9$, full duct), $K=0.36$ ($A_3/A_1=1.9$, half duct), $K=0.45$ ($A_3/A_1=3.75$), $K=0.4$ ($A_3/A_1=6.6$).

5. Comparison with 1D Model

A comparison was made of the CFD calculated values for C_p and those calculated using the 1D model. The parameters η_{01} and η_{23} were used along with an extra multiplier a to take account of other factors which may reduce the performance of the duct, e.g. flow asymmetry and the effect of the building, such that:

$$C'_p = aC_p \tag{8}$$

where C'_p is the performance coefficient adjusted for factors which reduce the overall performance of the duct, to give the best fit of the 1D model to the CFD calculations. In addition, because there is off-axis flow into the duct which cannot be modeled by the 1D theory, η_{01} is assumed to be divided by $\cos(\theta)$ where θ is the angle that the flow makes to the horizontal on entering the duct. The values of $\eta_{01}/\cos(\theta)$, η_{23} and a determined using an iterative best fit, along with the base pressure drop coefficient C_{pb} determined from the CFD model are shown in Table 1. The value of η_{23} for the contraction ratio $A_3/A_1=1.9$ is broadly in line with the observations in [17]. The values for other contraction ratios are out of the range of observations in [17]. Assuming that η_{01} would be close to 1 for an efficient inlet, then θ would appear to be around 37° which is not inconsistent with the streamlines entering the duct in Figure 3 (a) and (b). The a parameter ranges for 0.75 to 1 for contraction ratios $A_3/A_1=1.9$ to $A_3/A_1=6.6$, respectively. This reflects the largest degree of separation for the lower contraction ratio case. This is to be expected as the flow has to be turned through 90 degrees with the sharpest angle for the lowest contraction ratio duct compared with the highest contraction ratio. Higher contraction ratios also cause greater flow acceleration in the inlet, eliminating local adverse pressure gradients in the boundary layer of the duct inlet and preventing flow separation.

As a base case, a CFD run was done for the $A_3/A_1=1.9$ contraction ratio with no building, i.e. for a free-standing duct, and the parameters in the 1D model adjusted accordingly for the best fit. These results are shown in Table 2. It can be seen that $\eta_{01}/\cos(\theta)$ is 1 corresponding to a perfectly ‘swallowing’ duct with no appreciable off-axis flow in this case. The pressure drop in the diffuser is in line with [17] where η_{23} is 0.9 as for the building mounted case. The magnitude of the base pressure coefficient is lower than the building case as expected. No reduction in overall duct performance is apparent, i.e. $a=1$ as would be expected.

Finally, the half-span duct CFD results were compared with the 1D model adjusting the parameters as before. It can be seen that for low resistances the overall duct performance parameter a is quite low (0.5). As the resistance is increased, the parameter a increases up to an apparent value of 0.97 for the highest resistance value. This is consistent with Figure 4 (a) and (b) where the streamlines show a large degree of separation for the low resistance case and virtually no separation for the high resistance case.

A_3/A_1	$\eta_{01}/\cos(\theta)$	η_{23}	a	C_{pb}
1.90	1.25	0.9	0.75	-0.1
3.75	1.25	0.95	0.9	-0.1
6.60	1.25	1	0.95	-0.1

Table 1: Parameters in 1D model to give best fit to CFD calculations for ducts of varying contraction ratio on building.

A_3/A_1	$\eta_{01}/\cos(\theta)$	η_{23}	a	C_{pb}
1.90	1	0.9	1	-0.06

Table 2: Parameters in 1D model to give best fit to CFD calculations for $A_3/A_1=1.9$ for a free-standing duct (no building).

K (half)	$\eta_{01}/\cos(\theta)$	η_{23}	a	C_{pb}
0	1.25	0.9	0.5	-0.4
0.36	1.25	0.9	0.5	-0.4
0.68	1.25	0.9	0.5	-0.4
0.98	1.25	0.9	0.65	-0.4
1.29	1.25	0.9	0.97	-0.4
1.6	1.25	0.9	0.97	-0.4

Table 3: Parameters in 1D model to give best fit to CFD calculations for the $A_3/A_1=1.9$, half-span duct. Note that the a parameter varies as resistance K is increased.

6. Discussion

The performance of a wind turbine rotor within a free-standing duct is clearly different to that where the duct is mounted on top of a flat-roofed building. The building itself creates a significant acceleration of the flow as it approaches and moves over the top of the building. The flow separates where it hits the leading edge of the building, though this separation point will be displaced upwards by the addition of the duct then occurring at the top edge of the duct.

Designing the inlet to the duct in order to maximise its ‘swallowing’ efficiency is not trivial and it is difficult to separate out the efficiency of the inlet from the speed-up effect of the building. There is a significant vertical component to the flow close to the building and designing an inlet capable of directing that flow horizontally whilst avoiding flow separation is difficult.

One significant difference between the free-standing duct and the building-mounted arrangement is the asymmetry seen in the vertical profile within the duct and an adverse pressure gradient in the lee of the building and above the building due to the flow separation bubbles. This produces loss in performance even at low contraction ratios (small diffuser angles) for the building-mounted case compared with the free-standing duct as flow separation is seen at the bottom of the duct. These facts make determination of diffuser efficiencies from the 1D model problematic. Indeed, it is not obvious that the diffuser inlet and outlet efficiencies can be treated as independent of the rotor resistance.

A half-span duct has the potential to reduce material costs but seems to exhibit significant flow separation at low rotor resistance resulting in loss of performance. However, as the rotor resistance is increased, performance seems to improve and approach that which might be seen for the free-standing case. This would seem to be due to the rotor forcing the flow towards the edges of the duct and so inhibiting flow separation. This observation is consistent with the experimental findings described earlier in [10].

7. Conclusions

A comparison has been made between the performance of a building-mounted ducted wind turbine as predicted from 1D theory and calculated using a CFD code in 3D. When comparing results for a free-standing duct, agreement between the 1D theory and simulations is good. However, in the building-mounted case, deviations from the 1D results are apparent and would seem to be due to:

- The acceleration effect of the building;
- Vertical flow asymmetry within the duct affecting the diffuser performance;
- Building-induced separation effects affecting both the inlet and diffuser performance.

It is interesting to note that when simulating the performance of a shortened duct (not spanning the entire length of a building), that at low rotor resistance performance is poor, but as rotor resistance is increased, so performance increases approaches that of a free-standing duct.

Though the advantage of the CFD simulations is to provide some insight into the patterns of flow and possible reasons for the change in performance of the duct in different configurations, field testing measurements would be required to validate the conclusions of this work. Nonetheless the results presented here give some insight into the performance of a building-mounted ducted wind turbine and provide an indication of how a simple 1D theory might be empirically corrected to account for the effect of mounting the duct on a building.

References

- [1] Renewable Devices Swift Turbines Ltd (2007), 'SWIFT Rooftop Wind Energy System™', information sheet published by Renewable Devices SWIFT Turbines Ltd.
- [2] Windsave, <http://www.windsave.co.uk>, last accessed 25th May 2007.
- [3] Mertens S (2002), 'Turby', University of Technology Delft, DUWIND report 009.
- [4] Urban Wind Energy, <http://www.urbanwindenergy.org.uk/index.asp?PageID=84>, last accessed 25th May 2007.
- [5] Mertens S (2006), 'Wind energy in the built environment', ISBN: 0906522358, Multi-Science, Brentwood, Essex, UK
- [6] Heath M A, Walshe J D and Watson S J (2007), 'Estimating the potential yield of small building-mounted wind turbines', *Wind Energy* **10**, pp 271-287.
- [7] Watson S J, Infield D G and Harding M R (2007), 'Predicting the performance of small wind turbines in the roof-top urban environment', *Proc. European Wind Energy Conference*, 7th-10th May 2007, Milan, Italy. To be published.
- [8] Lawn, C J (2003), 'Optimization of the power output from ducted wind turbines', *Proc. Instn. Mech. Engrs*, **217**, Part A: J. Power and Energy, pp 107-117.
- [9] Matsushima T, Takanewagi S and Muroyama S (2006), 'Characteristics of a highly efficient propeller type small wind turbine with a diffuser', *Renewable Energy* **31**, pp 1343-1354.
- [10] Abe K and Ohya Y (2004), 'An investigation of flow fields around flanged diffusers using CFD', *J. Wind Engineering and Industrial Aerodynamics* **92**, pp 315-330.
- [11] Abe K, Nishida M, Sakurai A, Ohya Y, Kihara H, Wada E and Sato K (2005), 'Experimental and numerical investigations of flow field behind a small wind turbine with a flanged diffuser', *J. Wind Engineering and Industrial Aerodynamics* **93**, pp 951-970.
- [12] Grassman H, Bet F, Ceschia M and Ganis M L (2003), 'On the physics of partially static turbines', *Renewable Energy* **29**, pp 491-499.
- [13] Dannecker R K W and Grant A D (2002), 'Investigations of a building-integrated ducted wind turbine module', *Wind Energy* **5**, pp 53-71.
- [14] Rhie C M and Chow W L (1983) 'Numerical study of the turbulent flow past an airfoil with trailing edge separation', *AIAA J* **21** pp 1527-1532.
- [15] Menter F R (1993) 'Zonal two equation k- ω turbulence model for aerodynamic flows', AIAA paper 93-2906.
- [16] Launder B E and Spalding D B (1972), 'Mathematical models of turbulence', Academic Press, New York.
- [17] Ward-Smith A J (1980), 'Internal fluid flow', Clarendon Press, Oxford.